



Cite this: *Catal. Sci. Technol.*, 2024,
14, 515

Received 19th August 2023,
Accepted 1st December 2023

DOI: 10.1039/d3cy01160g

rsc.li/catalysis

The design and optimization of heterogeneous catalysts using computational methods

Shambhawi,^a Ojus Mohan, Tej S. Choksi and Alexei A. Lapkin *^{ad}

The computational design of catalytic materials is a high dimensional structure optimization problem that is limited by the bottleneck of expensive quantum computation tools. Current implementations of first principles computational models for catalyst design are data-hungry, problem-specific and confirmatory in nature. However, they can be made less data-dependent, more transferable and exploratory by developing both forward and inverse catalyst mapping tools that are either inexpensive correlations, like scaling relations, or regression models that are based on relevant descriptors analysis. This work reviews the current application and the possible landscape for future advancements of such tools for developing generalized schemes for catalyst design and optimization.

1. Introduction

Today heterogeneous catalysis facilitates highly energy-efficient selective molecular transformations for over 90% of the chemical manufacturing processes and contributes towards 20% of all industrial products.^{1,2} Given the importance of heterogeneous catalysts in chemical processes, developing rational heterogeneous catalyst design rules is one of the most fundamental goals in reaction engineering and is the key towards developing future sustainable chemical technologies. However, catalyst design is a complex process, involving numerous interacting factors, such as active species (metal, oxide, *etc.*), promoter, support type, preparation method, and pre-treatment conditions, see Fig. 1. Any variation in these factors can cause significant changes in activity and selectivity of the catalyst. The same is true for the operating conditions: different combinations of reaction variables such as temperature, feed flow rate, and feed composition.³ Because of the multidimensional complexities, theoretical catalyst design has limited application in material exploration for catalyst development, whereas trial and error and repeated experiments are still the main strategies. Another major challenge associated with computational approaches is the disassociation of their performance evaluation metrics from real catalyst compositions,

like obtaining a 3D structure of a synthesizable material as an output, from an inputted rate or selectivity.

With the development of computer-aided data storage and processing techniques, vast amounts of accumulated knowledge on catalysts can be employed in analysis simultaneously.³ Additionally, the multidimensionality of the catalyst design problem can be represented in a machine readable format for developing prediction models. For example, ML algorithms have been trained on data corresponding to catalyst performance metrics (*e.g.* % reactant conversions,^{4,5} product yield or turnover frequency,^{4,6} key reaction energetics^{7–9}), produced from high-throughput experimentation or computation coupled with a combinatorial algorithm, to predict catalyst materials with the best performance. They have also been used to construct inverse functions, *i.e.* mapping from properties to materials¹⁰/molecules.¹¹ However, accuracy of predictions of these models is limited to the training set distribution, specifically, catalytic structures, composition variations and binding molecules. On the other hand, graph-based representations coupled with neural networks are used for a more generalized implementation, *e.g.* predicting energetics over a catalyst surface for subsequent micro-kinetic modelling.¹² However, their data requirements can be two orders of magnitude higher than other simpler regression algorithms.¹³

Developing a generalized design scheme for heterogeneous gas-phase reactions that is computationally effective, accurate, and transferable (valid for different reaction systems and catalyst compositions), without relying on data-heavy techniques, is among the major research goals in catalysis. In this review, we discuss the implementation of popular theoretical tools, approaches and workflows used in materials investigation for catalyst screening and optimisation under the listed constraints. We compare their applicability for different

^a Department of Chemical Engineering and Biotechnology, University of Cambridge, Cambridge CB3 0AS, UK. E-mail: aal35@cam.ac.uk

^b Chemical Engineering Department, Indian Institute of Technology Bombay, Powai, Mumbai, Maharashtra 400076, India

^c School of Chemistry, Chemical Engineering and Biotechnology, Nanyang Technological University, 62 Nanyang Drive, 637459, Singapore

^d Cambridge Centre for Advanced Research and Education in Singapore Ltd, 1 Create Way, CREATE Tower #05-05, 138602, Singapore



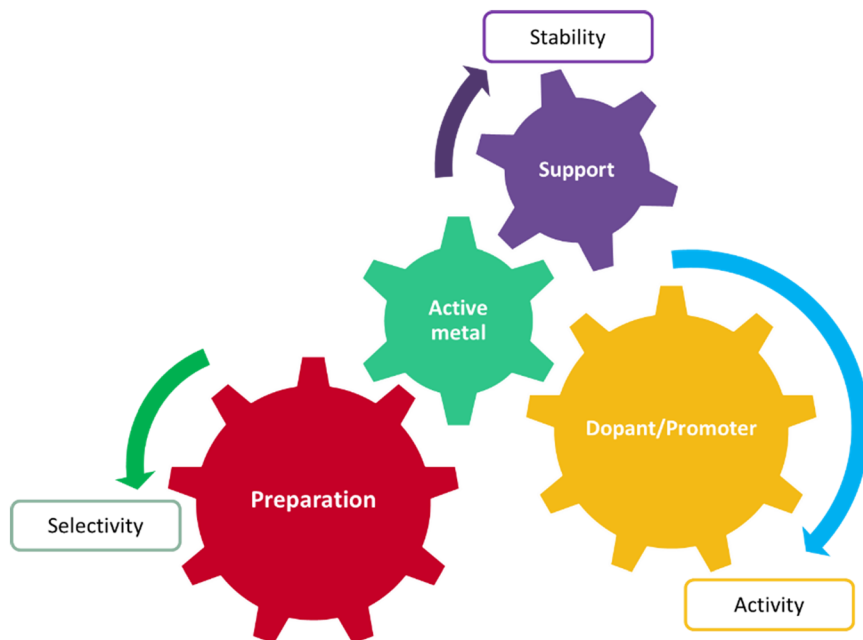


Fig. 1 Different factors involved in the design and optimisation of a catalyst material.

problem systems while highlighting the recent advancements made in order to bypass the current computational bottleneck in catalyst design. We start with the tools used for computing reaction energetics over catalysts surfaces. These tools include first-principles methods, their semi-empirical/empirical adaptations and molecular dynamics. We compare different methods reported in the literature for developing reaction networks, catalyst optimization and screening. Lastly, we summarize state-of-the-art in theoretical catalyst design and discuss its potential future landscape based on the existing developments.

2. Reaction chemistry computation

The kinetics on a given catalyst surface are driven by the energetics of elementary steps occurring on active sites. In this section, we discuss the most common approaches for computing reaction energetics (adsorption energies, activation barriers) over catalyst surfaces. Density functional theory (DFT) is the most popular choice for quantum mechanical computations. Other tools are essentially semi-empirical/empirical implementations derived from or trained on DFT but are relatively less expensive. This also includes tools for molecular dynamics. We further compare them based on three key factors: transferability, accuracy, efficiency, applicable system size, and highlight their respective limitations, see Table 2.

2.1 Quantum mechanical calculations and density functional theory (DFT)

In the realm of reaction chemistry computation, quantum mechanical calculations have emerged as indispensable tools.^{14–17} These calculations have revolutionized our

understanding of the behavior of atoms, molecules and materials by providing insights into their electronic structure and properties at the microscopic level. Hartree–Fock (HF) calculations are one of the oldest quantum mechanical methods based on wavefunctions that is used to study electronic structure.^{18–20} They are based on a self-consistent field approach, where the electrons are treated as non-interacting particles within the mean field generated by the other electrons. While HF calculations provide a good starting point for understanding the electronic structure, they have limitations, particularly in accurately describing electron correlation effects.¹⁹ Several post-Hartree–Fock methods have been developed to account for electron correlation effects beyond the HF level. Examples include configuration interaction (CI),²¹ coupled cluster (CC),²² Møller–Plesset perturbation theory (MP2),²³ and density functional theory (DFT).^{24,25} These methods offer improved accuracy by including electron correlation contributions, but some of them can be computationally demanding, especially for large systems. Among the post-Hartree–Fock methods, density functional theory (DFT) is the only method based on density function instead of wave functions. It has become a widely employed computational tool for studying the electronic structure and reaction energetics, especially for catalytic systems.²⁶ It offers a versatile framework to investigate a wide range of systems and phenomena.

DFT is a widely used method for electronic structure calculations. At the core of DFT calculations is the concept of electron density. Instead of solving Schrödinger equation for the system's wave function, DFT focuses on determining the electron density distribution, which is a more tractable quantity.^{24,25} This approach has proven to be highly effective in studying a wide range of catalytic systems.²⁶ The most



widely used form of DFT is Kohn-Sham density functional theory (KS-DFT). It was proposed by Walter Kohn and Pierre Hohenberg in 1964 and has become the cornerstone of modern DFT calculations.^{24,25}

The Kohn-Sham approach introduces a set of auxiliary non-interacting electrons, represented by Kohn-Sham orbitals, to approximate the real system's electron density.^{24,25} These orbitals are derived from a fictitious system in which the electron-electron interactions are neglected. However, the electron density obtained from the Kohn-Sham orbitals should match the electron density of the real system. In KS-DFT, the electronic structure problem is mapped onto a set of non-interacting electrons moving in an effective potential. To solve the Kohn-Sham equations, a basis set is used to expand the Kohn-Sham orbitals. The choice of the basis set is critical in accurately representing the electronic structure of the system.²⁷ The basis set represents a set of functions that span the space in which the electronic wave functions are defined. In KS-DFT calculations, the choice of a basis set and the package used to solve the equations depends on the nature of the system being studied: cluster/isolated system, bulk (periodic) system, or condensed media.

In cluster calculations, where a small group of atoms or molecules is isolated from its surroundings, the basis set is typically chosen to describe the electronic structure of the cluster accurately.²⁸ The commonly used basis sets in cluster calculations include Gaussian-type orbitals (GTOs).^{29,30} Gaussian,³¹ ORCA,³² and GAMESS³³ are widely used software packages for calculations involving cluster/isolated molecules.

In bulk or periodic system calculations, the electronic structure is determined for extended periodic structures such as crystals and surfaces. In these calculations, the basis set is expanded to include periodic boundary conditions.³⁴⁻³⁶ Plane-wave basis sets are commonly used in periodic system calculations, along with pseudopotentials or projector-augmented wave (PAW) potentials to efficiently treat the electron-ion interactions.^{36,37} Since the potential is periodic, the plane wave basis sets are well-suited for the description of periodicity in the crystal lattice. VASP,^{34,38} Quantum Espresso^{39,40} and CASTEP⁴¹ are popular packages for periodic DFT calculations.

Condensed media calculations involve studying systems where the electronic structure is influenced by the surrounding environment, such as liquids, solutions, or solids with embedded solvents. CPMD, which stands for Car-Parrinello molecular dynamics, is particularly useful for simulating condensed phase systems and exploring reaction mechanisms with atomistic detail.⁴² CPMD is a computational method that combines molecular dynamics simulations with DFT. CPMD utilizes plane wave basis sets to describe the electronic structure and employs the Born-Oppenheimer approximation to treat the nuclear motion.⁴² This approach allows for the study of dynamic processes, such as chemical reactions and materials transformations, at

the quantum mechanical level. In short, the choice of basis set in DFT calculations significantly impacts the accuracy and computational cost of the calculations. Larger and more sophisticated basis sets can provide a more accurate description of the electronic structure but at the expense of increased computational resources and time.

In addition to the selection of an appropriate basis set, one of the other major challenges in DFT is choosing an appropriate exchange-correlation functional, which accounts for the electron-electron interactions.^{43,44} However, the exact form of the exchange-correlation functional is not known. Many approximations exist for the exchange-correlation functional, and selecting an appropriate functional is crucial to achieve reliable results. Generalized gradient approximation (GGA)⁴⁵ functionals, such as PBE,⁴⁶ PW91,⁴⁷ and revPBE,⁴⁸ are commonly employed in DFT calculations. Benchmarking of functionals is necessary to ensure their reliability in DFT-based catalyst design procedures. For instance, many studies employ GGA-based PBE and PW91 functionals for studying CO₂ conversion reactions on solid catalysts. However, inconsistencies arise between the calculated values using these functionals and experimental data.⁴⁹⁻⁵¹ Notably, the binding energies of CO₂ on metal surfaces, often deviate significantly.⁵² Additionally, GGA functionals are inadequate for describing weakly bound systems, where dispersion interactions play a crucial role.⁵³⁻⁵⁵ Incorporating van der Waals (vdW) interactions through specific correlation functionals can improve the accuracy of dispersion-bonded systems.

The Hubbard U is yet another DFT parameter based on the Hubbard model (DFT+U method)^{56,57} that is crucial for accurately describing the electronic properties of transition metal oxides by employing DFT. Metal oxides, with their transition metal elements, exhibit strong electron-electron interactions and localized electron behaviour. Standard DFT functionals may not adequately capture these effects, leading to inaccurate predictions. The Hubbard U term represents the on-site Coulomb repulsion between electrons and helps describe the physical behaviour of transition metal oxides. Incorporating the Hubbard U parameter improves the agreement between DFT calculations and experimental observations, enabling accurate predictions of structural, electronic, and magnetic properties. Determining the appropriate Hubbard U value is challenging and often relies on empirical or theoretical approaches. By including Hubbard U, DFT calculations provide valuable insights into metal oxide properties, including bandgaps, energy levels, charge localization, and magnetic behaviour.^{58,59} The Hubbard U parameter is essential for understanding metal oxides' electronic structure and behaviour within the DFT framework. For further detailed overviews on DFT, its parameters and application we direct the readers to review articles in ref. 60 and 61.

Although DFT calculations are accurate and reliable for studying different reactions on a small set of catalysts, they cannot be directly applied to problems that require high



Table 1 The total computation time for computing the DFT energies for CO₂ methanation reaction on three different catalyst surfaces

Type of DFT calculation	No. of calculations	No. of cores	CPU time	Total core hours
Geometry optimization	600	64	5	192 000
Transition state searches (minimum energy path)	135	96	15	194 400
Transition state optimization	45	64	2	5760
Transition state confirmation <i>via</i> vibrational frequency	45	64	10	28 800
Adsorbate vibrational frequency	24	64	10	15 360
Grand total of core hours				436 320
Number of catalyst surface investigated (Ni(111), Ru(0001), NiB(111))				3
Total CPU (core years)				145

throughput computations, particularly in catalyst design problems involving the calculations of potential energy surfaces (PES) for reaction chemistry. Although the computational cost of determining minima in the PES is reasonable, determining the maxima (saddle points) can increase the computation time significantly depending on the number of images used. For complex systems like nanoclusters, single atom alloys (SAAs) and single-atom catalysts (SACs), this increase can be even higher.

Given that the method is based on first principles, it is transferable, but the accuracy is highly affected by the choice of functional and other computational flags. The speed/efficiency of the method is also way below the requirement for a comprehensive analysis. This can be observed from Table 1 that highlights the computational resources needed for evaluating reaction energetics over three catalyst surfaces for performance comparison for the CO₂ methanation reaction.

2.2 Density functional based tight binding method (DFTB)

The density functional-based tight binding method or DFTB was initially based on a second-order expansion of the DFT total energy with respect to charge density fluctuations.⁶² However, the most common implementation, DFTB₃,⁶³ includes a third-order expansion of the DFT total energy.

DFTB methods can be two-to-three orders of magnitude faster than *ab initio* and DFT.⁶⁴ They are particularly attractive in applications to large molecules and condensed phase systems and have already been implemented for geometry optimization of inorganic solid structures,⁶⁵ nanoclusters⁶⁶ and SACs.⁶⁷ DFTB has also been implemented for transition state searches for reactions involving large (bio)molecules.⁶⁸

However, without proper benchmarking, the accuracy of the method can be heavily compromised,⁶⁹ making the use of DFTB trade-off between speed *vs.* accuracy. Transferability of the model is also limited when heavy metal elements come into question.⁷⁰

2.3 Unity bond index-quadratic energy potential (UBI-QEP)

UBI-QEP is a generalization of the BOC-MP (bond order conservation-Morse potential) method that is used for modelling chemisorption energetics and reaction mechanisms on metal surfaces. It has a fast and easy computational implementation and the UBI-QEP projections of reaction

energetics are usually more accurate. It should be noted that the UBI-QEP modelling in particular is not competitive but complementary to quantum mechanical modelling.⁷¹ As input parameters, the method employs thermodynamic observables such as gas-phase bond energies and atomic chemisorption energies mostly obtained from DFT. Its output is the surface reaction energetics for all elementary steps in a mechanism thus improving the overall efficiency. Although these energies cannot be transferred to new adsorption systems without the initial DFT input.

The BOC-MP and the UBI-QEP methods have been applied successfully to analyse mechanisms of many reactions of practical importance such as methanol synthesis,⁷² Fischer-Tropsch synthesis,⁷³ and methane reforming chemistry on metal surfaces.⁷⁴ There are also UBI-QEP analytical formalisms for bimetallic surfaces however, similar developments cannot be found for systems like single atom catalysts and nanoclusters.

2.4 Reactive force fields (ReaxFF)

The reactive force-fields (ReaxFF)⁷⁵ are based on a bond-order formalism that implicitly describes chemical bonding without expensive quantum mechanical calculations. Its bond-order parameters are derived from computationally intensive DFT derived methods. Once these parameters are known, computing the energy matrix could be more than 100 times faster than DFT for gas-phase heterogeneous reaction systems. ReaxFF potential parameters have already been reported for hydrocarbons chemistry,⁷⁶ H₂ dissociation on transition metals,^{77,78} carbon interactions with transition metals⁷⁹ and lastly hydrocarbon reactions catalysed on transition metals such as nickel⁸⁰ and vanadium oxides.^{81,82}

In short, ReaxFF can model reactions at the gas-solid interface and assess the stability of SACs,⁸³ nanoclusters⁸⁴ and SAAs,⁸⁵ which is pertinent to our problem of heterogeneous catalysts design. Moreover, the available parameters for elements in the literature are also transferable, as long as the aqueous phase reactions are not involved.⁷⁵ However, proper benchmarking needs to be performed to determine the accuracy prior to any calculations and ReaxFF cannot be transferred to new systems without re-parameterizing the method.

The major drawback accompanying these force-field methods is the low accuracy of predictions which can be limited by proper parameterization of interatomic potentials. Recently there have been some developments in this area



Table 2 A comparison of different computational methods based on quantum mechanics, force field and molecular dynamics for generating reaction energetics in terms of transferability, accuracy, efficiency (speed) and applicable system size

Method	Transferability	Accuracy	Efficiency	Approx. system size (# atoms)
DFT	Based on first principles hence more transferable than the semi-empirical/empirical methods	Relative comparison of catalysts can be performed accurately Absolute catalyst predictions are also possible if the exchange correlation functionals are correctly identified using experimental data	Computational cost increases cubically with the increasing number of atoms in the system	10^2
DFTB	Limited for heavy metal systems	Benchmarking is required to compute the accuracy	Computational cost increases cubically with the increasing number of atoms. However each single point computation is 2–3 three orders of magnitude faster than DFT	10^3
UBI-QEP	Needs re-calibration in case of a new adsorption system (e.g., in presence of a new bond or a new element) Implementations limited to mono and bi-metallic catalyst systems	Accuracy depends on the DFT data used for calibration	Computational cost increases linearly with the increasing number of atoms	10^2
ReaxFF	The ReaxFF potentials need to be evaluated and validated every time a new element and/or is added to the adsorption system Not suitable for aqueous phase reactions	Benchmarking is required to compute the accuracy	Computational cost increases linearly with the increasing number of atoms	10^5 – 10^6

with the use of machine-learned (ML) force fields. These ML-corrected force fields have been found to be much more accurate. Further details on ML force fields can be found in section 5.1.4.

Table 2 summarizes the comparison of different quantum computational tools discussed here based on four the key factors: transferability, accuracy, efficiency and system size (number of atoms). There are additional methods in the literature that can be implemented to our problem of reaction chemistry computation but are not discussed here, *e.g.* MOPAC (Molecular Orbital PACKAGE) semi-empirical methods⁸⁶ or group additivity⁸⁷ used in automated reaction kinetics generation.^{88,89} For a comprehensive study, we refer our readers to other reviews that are focuses on these semi-empirical⁹⁰ and empirical methods.⁹¹

3. Reaction mechanisms generation

A reaction mechanism describes a network of elementary reactions (reaction network) which corresponds to the reaction coordinate from reactants to products and byproducts. The hypotheses about possible reaction intermediates and elementary reaction steps are based on experimental observations, literature-based dissociation and association routes, and/or auto-reaction generators algorithms⁸⁹ that employ reaction energy data,^{92–94} templates^{88,95} or heuristics. The methods for developing a reaction network can be broadly classified as:

- (1) Automated reaction mechanism generation that is based on reaction rates, and.
- (2) User-defined reaction rules for mechanism generation that are based on literature and experiments.

This section discusses the tools for developing reaction mechanisms *via* these approaches.

3.1 Automated reaction mechanism generation

An automatic reaction-mechanism generation (ARMG) is based on an algorithm that can perform the following tasks:⁸⁹

1. Recognize when two or more species in the mechanism are equivalent.
2. Predict all the possible elementary reactions for each species and pair of species.
3. Determine which of these possible reactions are important.
4. Estimate accurately all the necessary thermodynamic and kinetic parameters.
5. Ensure that the mechanism is thermodynamically consistent.

ARMG can be simultaneously used to update the reaction mechanism with catalyst surfaces during the optimisation of overall catalyst performance. This is particularly useful since reaction mechanism identification is based on the surface energetics over a catalyst. Therefore, surface energetics and by extension, the mechanism can vary from one catalyst to another.

A challenge with ARMG is determining the kinetically relevant reaction steps in the initial reaction network. A prior assumption about the list of intermediates and reactions can lead to biased results or limited solutions. If all possible intermediates and reactions are included, then the resulting reaction network quickly becomes unsolvable and, therefore, useless.



Gao *et al.*⁸⁸ developed an algorithm to circumvent this problem. The algorithm uses reaction rates to determine which species and reactions to include in the model. Reaction rates higher than a given tolerance are included in the reaction network and its corresponding reaction species are categorised as core species. It employs a thermochemistry prediction algorithm for rate evaluation. It uses a database of thermochemistry for known gas-phase species and surface species with group additivity and scaling relations (see section 5.2) respectively to predict the thermochemistry for new species. Goldsmith and West *et al.*⁸⁹ extended this tool for implementation in heterogeneous catalysis by adding an adsorption correction to the estimated gas-phase energy.

3.2 User-defined reaction rules to construct reaction mechanisms

Reaction networks can also be constructed using user-defined rules around a mechanism that is based on experimental evidence and literature. For example, Rangarajan *et al.*⁹⁰ constructed a reaction network for glycerol conversion using rules based on experimental evidence. The rules allowed the algorithm to include reactions that perform C–C, C–H, C–O, and O–H scission, C=O formation and further, C–H and C–O, and C–C formation. Several steps were not included because resulting intermediates were not reported in experimental studies.^{97,98}

This method can be categorized as reaction specific, partly intuitive and based on heuristics observed in the literature/experiments. The common framework is to look in the literature for elementary steps corresponding to reactant dissociation, product association and redox reaction steps in similar reactions with known mechanisms. For example, a study on methane reforming⁹⁹ copies the mechanism for dry reforming of methane (DRM) directly from CH₄ steam reforming with the addition of CO₂ dissociation steps. It is found that for small molecules reaction systems like DRM, the literature and automated mechanism generators agree on the same reaction network.^{89,99} There are also approaches in literature that automate the rule based reaction network generation¹⁰⁰ by including a language compiler that can convert an English-like reaction language into internal representations and instructions.

Designing a simple, yet representative reaction network is important for limiting the cost of evaluation and ensuring model solvability during mechanism identification and subsequent catalyst optimization. A way to achieve that would be *via* a partial reaction network made from relevant reaction species. A recent study¹⁰¹ outlines a workflow that can be used to create such partial reaction networks that are transferable across different catalyst surfaces and can be used for comparing catalyst activity performance.

4. Catalyst optimization

A reaction network and corresponding energetics observed over a catalyst surface are used for building kinetic models for evaluation of catalyst performance and their subsequent

optimization. There are top-down and bottom up approaches for building a kinetic model. The top-down kinetic model includes approaches based on power law expressions and Langmuir–Hinshelwood–Hougen–Watson (LHHW) mechanism. The assumptions in these approaches are more implicit. For example, assuming certain rate-determining elementary reactions, quasi-equilibrated elementary reactions, and the most abundant surface intermediates.¹⁰² Bottom-up approaches are theoretical models that do not make such initial assumptions about the nature of rate-determining elementary reactions but can be designed to enable different simplifications as per user requirements. This section discusses the theoretical bottom-up approaches used for quantifying catalyst performance.

4.1 Micro-kinetic modelling for optimizing catalyst surfaces

Micro-kinetic models (MKM) are a vital tool in catalyst research and design.¹⁰² Microkinetic models predict and compare the performances of different catalyst surfaces for a given reaction in terms of their reactivity, selectivity and stability against deactivation mechanisms like coking. MKMs are often designed and validated for a specific reaction system based on certain reaction conditions. As a result, complete MKMs are not adopted in subsequent studies, except for maybe certain model fragments, such as reaction networks and energy data. Different assumptions while creating an MKM also lead to different model predictions and the validity of these assumptions can vary. For example, using collision theory instead of transition state theory to model gas-phase adsorption, kinetic Monte Carlo instead of mean-field approximation to include the effect of surface coverage, and assuming quasi-equilibrium of certain reaction steps.

Regardless of the assumptions, formulating MKMs are computationally expensive. Subsequent catalyst design using MKM is therefore described as an expensive head-on approach for performance optimization. Fig. 2 shows MKM-

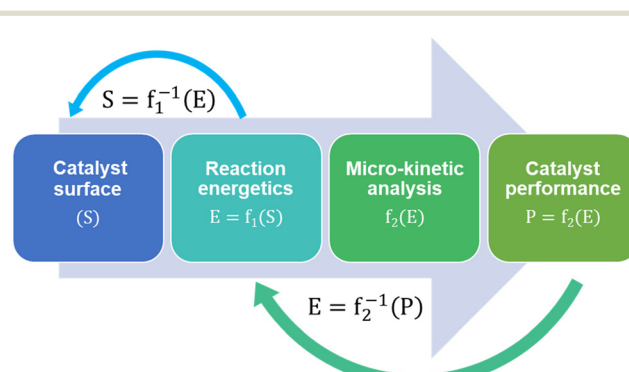


Fig. 2 A schematic of micro-kinetic model aided catalyst optimization *via* the expensive head-on approach. S corresponds to a structure matrix of the catalyst, E is the reaction energy matrix corresponding to intermediates and transition states, and P is the catalyst performance. f_1 represents the method for computing reaction chemistry for a given catalyst surface structure (S) and f_2 is the micro-kinetic model.

aided optimization of the catalyst surface for a reaction system in a step-wise manner:¹⁰³

- (1) An initial catalyst surface is fed into the micro-kinetic model.
- (2) Reaction energetics are computed based on thermodynamics.
- (3) The reaction kinetics are written followed by the reactor mass-balance equations.
- (4) The model is then solved to predict the corresponding catalyst performance.

The MKM-aided catalyst optimization employs the model to develop a function mapping between the catalyst structure and its performance. It then maximises the performance by closely studying the inverse function and its derivative,¹⁰³ *i.e.* f_1^{-1} and f_2^{-1} in Fig. 2.

The literature also reports another study¹⁰⁴ employing the MKM-aided catalyst optimization framework but in a less expensive inverse approach. The reaction energies are optimized independently, that is without subsequent optimisation of catalyst structure (see Fig. 3). Therefore, these energies correspond to a hypothetical catalyst that demonstrates improve catalytic performance and can be used for screening real catalyst materials. Although, the procedure for screening real catalysts is not elaborated.

The reaction energetics of a given reaction system can be very complex with interlinking energy values. A descriptor identification is important to make catalyst screening feasible. Herein, the descriptor would correspond to the energetics of the most relevant elementary reaction step (reader is directed to section 4.3 for further details).

4.2 Structure–activity/property mapping for screening catalyst materials

Contrary to the MKM-aided optimization approach, the quantitative structure–activity/property relationships (QSAR/QSPR) are based on developing a direct mapping between the microscopic (*e.g.* surface energies) and macroscopic properties

(*e.g.* reactant conversions) of a catalyst. In the case of heterogeneous catalysis, artificial neural networks (ANNs) are most used to develop this mapping for a given range of catalyst materials. The database used for training the ANNs are generated *via* high-throughput experimentation/simulations. The QSAR/QSPR¹⁰⁵ approach has already been implemented on different problems like materials screening, molecular design and synthesis. Their implementations for heterogeneous catalysis are also reported. Catalyst input features are usually the catalyst synthesis conditions and elemental compositions. However, depending on the adsorbate size, molecular descriptors can also be used to represent intermediates.

Despite the straightforward implementations of QSAR/QSPR, they are often limited to a specific problem system due to the lack of a diverse database, limited data points and reproducibility issues during experiments. A robust and reliable property prediction model is not possible if either of the following is true:

- (1) The experimental measurements have high uncertainties.
- (2) The chemical diversity beyond training sets.
- (3) The range of measured property values is too small.

4.3 Descriptor-based optimization of catalyst surfaces

The descriptor-based catalyst search is the most common approach towards theoretical catalyst optimization. It reduces the cost of exact model evaluation to descriptor evaluation and catalysts with descriptor values corresponding to maximum performance can be screened using the volcano plots¹⁰⁶ (reader is directed to section 4.3.3 for further elaboration on volcano plots). The overall optimization will depend on the chosen catalyst descriptors and is limited by the volcano plot relation, thus identifying relevant catalyst descriptors is a very important step for catalyst design. We discuss methods used to identify reaction descriptors, *i.e.* sensitivity analysis and reaction pathway analysis followed by a small introduction to volcano plots.

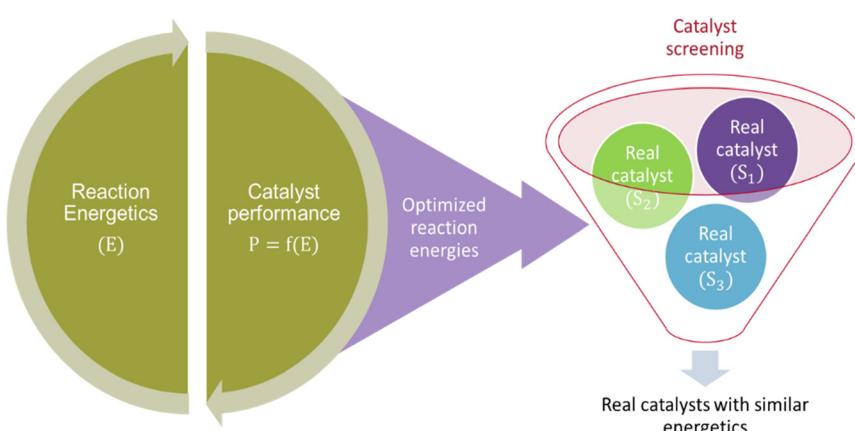


Fig. 3 A scheme of micro-kinetic model aided catalyst optimization *via* the inverse approach. E is the reaction energy matrix corresponding to intermediate and transition state energies observed over hypothetical catalyst intermediates and transition states, and P is the catalyst performance. f represents the micro-kinetic model framework. S_i corresponds to the structure matrix of real catalysts.



4.3.1 Sensitivity analysis. In this approach, the sensitivity of the catalyst's performance w.r.t. individual reaction steps/energies are evaluated (see eqn (1) and (2)).

$$X_{RC,i} = \left(\frac{\partial \ln r}{\partial \ln k_i} \right)_{K_i, k_j} \quad (1)$$

Eqn (1) corresponds to the degree to rate control (DRC).^{100,101} It is defined as the normalized partial derivative of the overall rate (r) w.r.t. the rate constant, k_i , while keeping the equilibrium constant, K_i and the rate constants, k_j of all other steps constant. A $X_{RC,i}$ value of zero indicates a reaction step, whose rate constant does not affect the overall rate, while $X_{RC,i} \approx 1$ indicates a rate-controlling step.

Although DRC is an extraordinarily useful concept for reaction mechanisms analysis, the energies of intermediates and transition states are linked through scaling relations (see section 5.2) and so are the rate constants. Thus, they cannot be changed independently during catalyst design. Therefore, instead of employing reaction energies with the highest DRC as catalyst descriptors, another metric is applied (eqn (2)), *i.e.* degree of catalyst control (DCC).¹⁰⁸

$$X_{CC,i} = \left(\frac{\partial \ln r}{\partial \frac{-E_i}{RT}} \right)_{E_i \neq j, BEP, Scaling} \quad (2)$$

where, $X_{CC,i}$ is defined as the degree of catalyst control and E_i is the reaction descriptor.

Based on the DCC, the activation/binding energy of the most sensitive reaction step/species is then chosen as the reaction descriptor. This descriptor is specific to the reaction investigated and can change if the reaction conditions are drastically changed.

4.3.2 Reaction pathway analysis. Reaction network and pathway analysis is a graph-based approach that is frequently used to identify highly interconnected intermediates and reaction steps that are solely connecting different reaction chemistries. Given a list of elementary reaction steps, reaction network construction of complex reactions outlines all available pathways for product formation. Further rate-based flux analysis on these pathways can be performed using algorithms, like Dijkstra's and variants,¹⁰⁹ to identify dominant pathways, respective contributions and rate-determining steps, *i.e.* relevant reaction descriptors.

4.3.3 Volcano plots. Volcano plots are based on Sabatier's principle,¹¹⁰ which states that a catalyst should bind a substrate neither too strongly, else it will destabilize the catalyst, nor too weakly, as that will reduce the activity. Thus, the maximum performance can be identified somewhere in between. The volcano plots provide an estimate of catalytic performance in terms of turn-over frequency, product yield or over potential, w.r.t. a descriptor variable, *e.g.* substrate binding energy, activation barriers. Developing these relations further requires reaction and transition state energies across catalyst surfaces ranging from highly reactive to inert. Recent efforts have led to the advent of databases (see section 5.1.2) that can be used to create these relations.

Despite its popularity, volcano plots limit the maximum attainable catalytic performance corresponding to bulk catalytic structures and cannot be generalized to structures like single atom alloys (SAAs) that are known for breaking the scaling relations based on bulk materials.^{111,112} They are also prone to error depending upon the linear scaling relation (see section 5.2) used in their construction. Section 5.2 highlights a specific scenarios where a deviation from volcano plots and scaling relations is observed. The reader is referred to ref. 112 for further details.

5. Catalyst screening

The ability to solve either the forward or the reverse optimization problems essentially boils down to the catalyst screening method. An ideal catalyst screening tool should be capable of performing high-throughput computation for a range of catalyst structures and composition variations.

In this section, we discuss the most common methods for inexpensive high-throughput screening of catalysts based on identified reaction descriptors, *i.e.* (1) machine learning for developing energy prediction models and (2) scaling relations as linear empirical relations for predicting reaction energies.

5.1 Machine learning (ML) models

Machine learning models can be employed to reduce the cost of reaction thermochemistry computation, thus enabling efficient catalyst screening. They can be trained on energies evaluated from DFT or other semi-empirical/empirical tools depending on the required accuracy and available data. ML models can be implemented at different stages in the overall computation. Implementations have been identified in the literature for predicting DFT wave functions or electronic density,¹¹³ predicting DFT energies¹¹⁴ and accelerating transition state searches.^{115,116} Further implementations include feature construction from relevant descriptors for initial catalyst screening¹¹⁷ and reactive force-fields parameters optimization for a more rigorous screening (see section 5.1.4).¹¹⁸

Given the inherent complexity of catalytic reactions, these machine learning-based implementations are relevant tools to efficiently navigate through this high-dimensional catalyst optimization problem. Although their performances rely on the training algorithm and feature sets, their predictions are not transferable beyond the training set. In the following sections, we list common catalyst features, available catalyst databases and learning algorithms used for developing these models.

5.1.1 Catalyst features. Heterogeneous catalysts for gas-solid reactions are exclusively inorganic materials derived from transition metals. Thus, relevant features for such materials can be identified based on the band theory of chemisorption. However, the following points should be considered when deciding on features for catalyst surfaces:¹¹⁹

(1) The features must be unique in representing the electronic and geometric structures of an active site.



(2) They must be easily computed or readily available from databases to enable rapid screening.

(3) They should be physically intuitive to ensure model robustness and direct inference of chemical insights.

Table 3 lists some of the primary features observed in the literature that were either used in feature construction or directly employed for predicting properties such as adsorption energies.

These primary features can be implemented directly or can be used to handcraft secondary features using dimensionality

reduction methods like LASSO, SISMO, etc. On-the-fly construction of these features has been a common approach for developing specific features for the set of catalysts relevant to the study. A generalized approach is to use a graphical representation of catalyst structures. Please refer to section 5.1.3 for more details.

From Table 3 it is noted that most of the site-specific features require an expensive *ab initio* calculation (e.g. bandwidth, band-filling, density of states, etc.). Moreover, these features are comparatively more important. Li *et al.*¹³⁷

Table 3 A summary of primary features for catalyst materials, as observed in the literature

Class	Name	Abbreviations	References
Stoichiometry	L^P	$\ x_p\ $	120, 121
Atomic properties of components	Atomic number	Z	114, 120, 121
	Atomic weight	A	114, 120, 121
	Group	G	114, 120–122
	Period	P	114, 120–122
	Mendeleev number	MN	120, 123
	Atomic radius	r_x	114, 117, 119, 121, 122
	Covalent radius	r_c, r_c^1, r_c^2, r_c^3	120–122
	van der Waals radius	r_{vdW}	—
	Pauling electronegativity	PE	114, 117, 119–122, 124–127
	Ionization potential	IP	114, 117, 119, 122, 124, 125
	Electron affinity	EA	117, 119, 122, 124, 125
	# s valence electrons	ν^s	120, 121
	# p valence electrons	ν^p	120, 121
	# d valence electrons	ν^d	117, 120, 121
	# f valence electrons	ν^f	120, 121
	Total # valence electrons	ν	120–122
	Magnetic moment/atom at 0 K ground state	m	120, 121
Bulk properties of components	fcc nearest neighbour distance	$bulk_{nnd}$	124
	Partial radial distribution function	$g_{\alpha\beta}$	128
	Radius of d-orbitals	r_d	117, 119, 124
	Radius of p-orbitals	r_p	129
	Coupling matrix element squared	V_{ad}^2	117, 119, 124, 126
	Specific volume	V_s	114, 120
	Band gap energy of 0 K ground state	E_{BG}	120
	Space group number of 0 K ground state	—	120
	Melting point	t_{MP}	114
	Boiling point	t_{BP}	114
	Enthalpy of fusion	ΔH_{fusion}	114
Surface	Work function	W	117, 119, 124, 126
	Cohesive energy	$E_{cohesive}$	125
	Surface energy	$E_{surface}$	114
Site	Number of atoms in ensemble	$site_{no}$	124
	Coordination number	CN, GCN ^a	124, 130
	Orbital wise coordination number	CN^α ($\alpha = s, d$)	131
	Bond-energy-integrated orbital wise coordination number	\overline{CN}^{sd}	129
	Nearest neighbour distance	$site_{nnd}$	122, 124
	d-band centre	ε_d	117, 119, 124, 126
	p-band centre	ε_p	132
	d-bandwidth	W_d, W_d^{mto}	117, 119, 124, 127
	d-band skewness	s_d	117, 119, 124
	d-band kurtosis	k_d	117, 119, 124
	d-band filling	f_d	117, 119, 124
	sp-band filling	f_{sp}	124
	Antibonding states (e _g) filling	f_{e_g}	133
	Density of d-states at Fermi level	DOS _d	124
	Upper d-band edge	ε_u	134
	Density of sp-states at Fermi level	DOS _{sp}	124
	Thermodynamic stability of active sites	BE _M	135
	Crude estimate of the property being predicted	—	136

^a GCN corresponds to the generalized coordination number. ^b W_d^{mto} is the d band center computed from muffin-tin orbital theory.



identified them as an important feature for his study on perovskites by performing a recursive feature elimination on a list of 66 features that included some of each atomic-specific, bulk-specific, surface and site-specific features. They also demonstrate a higher linear correlation with the binding energies of catalysts suggesting higher relevance.

Even so, these expensive *ab initio* features are not ideal features, given that one must perform a total energy DFT calculation to obtain them. To circumvent this, Andersen *et al.*¹²⁴ proposed a solution. Instead of computing the site-specific properties of surface atoms in diverse structures/compositions, the authors computed the site-specific properties of each site atom in their bulk phase and then averaged them. This model had a reasonable accuracy for predicting the binding energies of some common intermediates. However, this study only included multi-metallic catalyst systems whose structures are similar to the bulk-phase structure of the host metal, *i.e.* only a handful of atoms are replaced by a different metal atom in the bulk structure. It is difficult to implement the same model for catalyst compositions leading to a new structure entirely different from their respective bulk phase structure.

Noh *et al.*¹²⁷ and Li *et al.*¹³⁸ proposed a more prevalent solution. They used the semi-empirical tight-binding LMTO formulation developed by Harrison and Froyen¹³⁹ to evaluate interatomic coupled matrix element which was further used to derive site-specific properties. Noh *et al.* used the formulation to compute LMTO d-bandwidth and Li *et al.*¹³⁸ used it to compute an orbital-based coordination number. Li *et al.*¹³⁸ further reported that the models based on LMTO features performed same as the model based on expensive *ab initio* features. Noh *et al.*¹²⁷ claimed that LMTO d-bandwidths are an even better feature than d-bandwidths computed from expensive DFT. Harrison and Froyen's formulation¹³⁹ has been also extended to oxides and even f-block elements.⁷

5.1.2 Catalysts databases. Most of the studies employing ML-based reaction energy prediction models use in-house developed catalyst databases specific to the problem. This is because universal catalyst databases are difficult to realize given the enormous compositional and structural variations that are feasible. Even so, there are a few open-access databases that have been commonly employed across different studies and have consistently been improved to include more compositional and structural variations, see Fig. 4. Here we will discuss these catalyst databases, their key features and their limitations.

The CatApp database¹⁴⁰ includes reaction energies for approximately 3000 surface reactions on close-packed as well

as stepped fcc and hcp on the following metal surfaces; Ag, Au, Co, Cu, Fe, Ir, Mo, Ni, Pd, Pt, Re, Rh, Ru, Sc, V. All values have been calculated with the same code (DACAPO), the same exchange–correlation energy functional (GGA-RPBE⁴⁶). Therefore, one adsorption energy or reaction barrier can be compared to another with some confidence. The limitation of CatApp is that it does not store the atomic structures that are an output of the electronic structure calculations. Because of this data reproducibility is limited.

The Catalyst-Hub database¹⁴¹ contains more than 100 000 electronic structure geometries and results from more than 50 publications, including the ones present in the CatApp database. The datasets stem includes a direct link to their respective publications. The database contains a large variety of alloy surfaces and oxides. A large part of these reaction energies stems from the high-throughput study of chemical adsorption and hydrogenation on more than 2000 bimetallic alloy and pure metal surfaces.¹⁴² The calculations are performed using different tools and functionals and, hence, cannot be directly compared. However, the geometries could easily be used to re-compute the energies as per requirement.

The Open Catalyst database (OC20)¹⁴³ is the most recent and comprehensive database that is inclusive of previous databases and has further calculations based on the Materials Project database¹⁴⁴ that are consistent in their computation parameters like the DFT functional. OC20 consists of 1 281 121 density functional theory (DFT) relaxation calculations for 5243 different material compositions and 82 different adsorbates (small adsorbates, C1/C2 compounds, and N/O-containing intermediates). Although the adsorption energies most likely do not correspond to the lowest energy configuration.

It should be noted that despite the knowledge accumulation over the years for creating heterogeneous databases, they are far from being representative of the vast number of possible catalytic systems. Even the most recent OC20 database seems to include only 18.9% of the total systems and only 0.07% of the possible calculations.¹⁴³ Databases are also biased in the sense that they mostly include systems that have been considered hot by the computational heterogeneous catalysis community.

Materials Project¹⁴⁵ is another notable database that was constructed to accelerate material property investigation in general but also guides catalyst structure investigation. It has structural and *ab initio* data available for over 33 000 inorganic compounds that can be used to construct catalyst surfaces, define catalyst search spaces and also evaluate relevant features for machine-learning-based model predictions of intermediate binding energies.¹⁴⁶

In addition to these databases, there are also several studies^{114,127,137,146} that have published data on intermediate binding energies, mostly CO* and H* adsorption energies. Although these data are mostly specific to their corresponding catalytic systems under consideration.

5.1.3 Training algorithms. The learning algorithms for ML prediction models are selected based on the training set



Fig. 4 An illustration of a timeline of development of catalyst databases.



distribution and size. Training set size is often the limiting factor given the expensive data point evaluations. Most of the studies employ problem-centric databases where compositional variations are very limited, and catalysts are structurally similar with defined binding sites. Catalyst features, as shown in Table 3, can then be used for developing ML models using different regression algorithms *e.g.* ridged regressions,^{127,147} decision tree regressions,^{7,114,147} polynomial regressions,^{147,148} neural networks,^{127,147} Gaussian process regression,¹⁴⁹ *etc.* The better-performing algorithms are identified by testing their performance on validation sets.

There are structural variations within the same catalyst composition and stable binding sites could also be different on the same surface depending on the adsorbate. To incorporate these variations, graph-based representations of catalyst surfaces have been developed.^{8,150} These representations do not require extensively handcrafted features (*e.g.* d-bandwidth) and can be generalized to different structures and compositions (beyond d-band elements). Although the learning algorithm is not limited to the ones compatible with graphical input data. Graphs can be vectorized to employ different regression algorithms, but the process eventually reduces the information present in a graphical representation, thus, forcing us back to some kind of handcrafted features.

Convolution neural networks (CCNs) and variants¹⁵¹ are the most common approaches for preserving this information along the different training layers of neural networks and are found to outperform other implementations.¹⁵⁰ However, these models have a huge data requirement, more than 10^4 data points for a single adsorbate. These limitations bring us to the different training algorithms that have been specifically developed for these scenarios.

Active learning. Active learning is a user-interactive learning technique that is applied in cases where obtaining data labels is expensive. The algorithm identifies new training data dynamically based on a query strategy. The technique is helpful in the effective utilization of resources for data point evaluation and model training. It is found to increase the model prediction RMSE of binding energies from 0.18 eV to 0.05 eV and from 0.65 eV to 0.4 eV in bi-metallic systems¹²⁷ and perovskites respectively.⁷ Active learning algorithms have also been employed on datasets consisting of in-house generated data coupled with the above-mentioned available databases.^{127,146} Although there is a drawback to this supervised learning technique, *i.e.* estimating the actual prediction accuracy of the model using batch sampling. Increasing the batch sampling size narrows the confidence interval for actual prediction accuracy but increases the data requirement simultaneously.⁷

Transfer learning. Transfer learning is a popular technique where a model trained on one task is re-purposed on a second task, *i.e.* the model hyper-parameters are constant when transferring from one task to another thus reducing

the training data required for the new task. This is mostly implemented for deep learning models where data requirements can be significant, although, implementation for regression models like decision trees¹⁵² and Gaussian Process¹⁵³ can also be found. Transfer learning is an effective tool when computing binding energies of related adsorbates (*e.g.* C* and CH_x*) on catalyst surfaces. Although its applicability should be restricted to problems with limited data availability, else it could lead to the overfitting of output-layer hyper-parameters.

5.1.4 Machine learned force-fields (MLFFs) and training workflow. ML-based force fields are one of the many applications of ML in heterogeneous catalysis for evaluating free energy values and generating reaction mechanisms. They are developed to bridge the gap between the accuracy of *ab initio* methods and the efficiency of classical force fields.¹⁵⁴ MLFFs make physically motivated assumptions about the interatomic potentials, such as locality and smoothness of the potential energy surface (PES). However, unlike the empirically fitted force fields, they do not make any prior assumptions about the specific functional form of the PES as a function of the atomic positions.¹⁵⁵ Instead, any and all such information is extracted directly from a large set of input data that is used to develop these machine learned potentials. This data is computed at an accurate and computationally much more expensive reference level (commonly, DFT). Once the potential has been fitted, ML potentials can provide fast and accurate surrogate models of the DFT PES. It can be used to predict energies and forces for larger ensembles of atoms, without the need for additional reference data.

An ML potential can be generated for a given material using a database of reference structures (see section 5.1.2), a mathematical representation of the atomic structure and a regression model.¹⁵⁵ The representations are based on the local environment of the active site, centered on an atom and encoding information about its neighbors, ranging from simple two- or three-body terms all the way to complex “many-body” formalisms. The most commonly used representation is the “smooth overlap of atomic positions” (SOAP) as a many-body descriptor.¹⁵⁶ The regression approaches, on the other hand, can be either artificial neural networks (NNs), kernel-based methods or linear regression.^{154,155}

Recently ML-based interatomic potentials have been actively generated for elements in different bonding states^{157–159} including long range interactions.¹⁶⁰ Studies have also been focusing on developing a training workflow for rapidly generating machine-learned force fields (MLFFs) for investigating reaction mechanisms over catalyst surfaces. These workflows are automated and iterative where the training set eventually expands using different adaptive sampling and/or query strategies.^{154,161} The accuracy of reaction energetics predicted *via* these MLFFs is claimed to be as low as 0.05 eV (ref. 161) of those obtained through density functional which is quite remarkable.



5.2 Scaling relations

Scaling relations are theoretical constructs derived from the d-band model¹⁶² that relates the binding energies of a wide variety of catalytic intermediates to atomic adsorption energies for a range of catalyst surfaces.¹⁶³ There are two types of scaling relations in heterogeneous catalysis: thermodynamic scaling relations^{162,164} which describe correlations between adsorption properties of chemically related species (e.g. CH_x and C) and Brønsted–Evans–Polanyi (BEP) relations¹⁶⁵ that is a linear correlation between activation energies and reaction enthalpy.

The development of scaling relationships has provided a rigorous theoretical basis for enabling automate reaction mechanism generation (see section 3.1), identifying independent catalyst descriptors (see section 4.3.1) and further developing volcano plots (see section 4.3.3) for catalyst screening based on DFT calculations. These relationships are extensively used for heterogeneous reactions on monometallics,¹⁰⁶ bimetallics,^{166,167} oxides,¹⁶⁸ and metal/support interfaces¹⁶⁹ and have even been extended for application in nanocatalyst developments.¹³⁵ Scaling relations only require a handful of data point evaluation (approx. 20–30 data points) and can thus be developed on the fly for screening catalysts or even assessing the formation of nanocatalysts and SAAs.

It should however be noted that scaling relations with prediction errors beyond 0.2 eV are not considered appropriate for facilitating predictions, especially when using scaling relations consecutively, *e.g.* employing BEP relations that were developed over thermodynamic scaling relations.

5.2.1 Deviation from scaling relations and volcano plots.

Volcano plots arise from correlations in reaction energetics, known as scaling relationships. They were first reported for the NH_3 synthesis reaction¹⁷⁰ and have since guided many material searches. However, there could be deviations from the known scaling relations and volcano plots under the scenarios listed in ref. 112. In this article, we focus on the single atom alloys and high entropy alloy catalysts that can deviate from the scaling relations due to several reasons.

Adsorbing intermediates prefer to coordinate to a metal surface. Sometimes the need for higher coordination of adsorbate could lead to spillover to host metal, *i.e.* the minimum binding energy configuration occurs at the host site. This can lead to a deviation in the binding energy that breaks the scaling relation. This spillover phenomenon has been investigated in detail in ref. 111. It was observed that SAAs followed a unique linear BEP scaling relation (different from the bulk catalyst) when there is no spillover. However there is no discernible linear relations in the occurrence of a spillover onto the host.

There are also other factors reported in literature¹¹² that could cause a deviation from volcano plots and scaling relation predictions. For example, intermediates adsorbed over high entropy alloys experience site-specific Pauli repulsion interactions that can lead to deviations from

scaling relations.¹⁷¹ We refer readers to ref. 112 to further explore different factors causing deviation from volcano plots and scaling relation predictions.

5.3 Summary

The reviewed ML models and scaling relations are developed using data points generated from either DFT or DFT-based semi-empirical/empirical methods. They have been found to demonstrate reasonable accuracy and can be used for high-throughput screening of catalyst materials based on reaction energetics. They can also be developed for mapping material compositions that demonstrate the required activity, stability and selectivity for a given reaction system. However the corresponding property descriptor needs to be identified, for example using convex hulls to assess thermodynamic stability of catalyst materials.¹⁷² Their implementation can be both exploratory and confirmatory in nature, depending on the descriptor's applicability.

6. Conclusions

This review discusses different state-of-the-art tools that allow to bypass the current challenges in catalyst design, screening and optimisation. Starting with the computational bottleneck, *i.e.* obtaining reaction energetics, semi-empirical/empirical quantum chemical and molecular dynamics tools, *i.e.* DFTB, UBI-QEP, and ReaxFF have been developed. They can provide two-three times faster execution than DFT depending on system size and have been implemented for different problem systems in the literature. Their implementations are decided based on the required computational efficiency, transferability, accuracy, and applicable system size. There is always a trade-off between efficiency on the one side and transferability and accuracy on the other side. For example, ReaxFF can be implemented in a catalytic system for faster evaluation of reaction energetics, however, it cannot be transferred to another system without undergoing DFT parameterization. Likewise, there are set approaches for developing reaction networks and identifying reaction mechanisms. The obtained reaction networks are most likely based on literature evidence and heuristics, however, recent advancements have been made to automate the entire process using network analysis and intermediate scaling relations.

Once the reaction network is known, there are different approaches for theoretical catalyst optimization *via* micro-kinetic modelling, *i.e.* the direct and the inverse approaches. Most of the studies on catalyst optimisation focuses on identifying relevant descriptors that scale energetics with performance, circumventing the computational bottlenecks. Methods for such descriptor identification are based on sensitivity analysis, degree of rate control and degree of catalyst control, and reaction network/pathway analysis. Recent investigations have reported that descriptors identification over a given reaction system might not be transferable over different



catalyst surfaces, due to significant variation in energetics. In such scenarios, descriptors are strictly identified for a set range of varying energetics, beyond which they are not applicable.

Identified descriptors can be used for quick screening of relevant catalysts materials. However, high-throughput computational screening of catalysts can be elusive because descriptor evaluation is expensive, especially when the descriptor corresponds to activation barriers rather than binding energies and the material search space is large. However, inexpensive screening tools based on machine learning, secondary descriptors and on-the-fly scaling relations can be developed to solve this problem. ML models in particular have a range of implementations in heterogeneous catalysis, *e.g.* wave-function prediction, energy prediction and transition state searches. The availability of databases like Open Catalyst 2020, further makes their implementation more feasible.

Although, it should be noted that these databases only represent 18.9% of the total possible compositions and the perfect universal catalyst database does not exist. This is where ML techniques like active learning and transfer learning become relevant. These techniques are implemented for minimizing the number of expensive data evaluations, whereas the later focuses on bridging the accuracy of *ab initio* methods and efficiency of molecular dynamics using minimum data points. Additionally, on-the-fly scaling relations are also a feasible option as they only require a handful of data point evaluations and can be implemented for fast screening. In short, current approaches for developing a generalised catalyst design scheme can circumvent the computational bottlenecks. However, individual heterogeneous catalytic studies should be more inclusive of the bigger problem, knowledge accumulation, database contributions and generalization of findings including those of prediction models. Conscious efforts should be made to make reaction data more accessible and reproducible. We hope this review promotes better practices in this regard.

Another challenge associated with catalyst design is the functional mapping between the required rate/selectivity and the material composition in 3D. Scaling relations and generative ML have been found to be relevant tools for screening materials and asses their synthesizability based on stability factors like convex hulls/machine-learned accelerated molecular dynamics. A potential future catalyst design approach, therefore, combines multiple ML models and provides a list of candidate 3D structures with their stability/rates/selectivity/synthesizability scores.

We are still some way away from this scenario as individual segments of such a workflow are in place, *i.e.* preliminary screening based on catalyst performance descriptor, further proof of concept, *i.e.* combining generative models with synthesizability checks are in development to further guide advancements in theoretical catalyst design and optimisation.

Conflicts of interest

There are no conflicts to declare.

Acknowledgements

Shambhawi acknowledges the research scholarship funding from Science and Engineering Research Board, India and Cambridge Trust. This work was in part supported by National Research Foundation (NRF), Prime Minister's Office, Singapore under its Campus for Research Excellence and Technological Enterprise (CREATE) program as a part of the Cambridge Centre for Advanced Research and Education in Singapore Ltd (CARES), and Engineering and Physical Sciences Research Council *via* project EP/S024220/1 EPSRC Centre for Doctoral Training in Automated Chemical Synthesis Enabled by Digital Molecular Technologies. OM acknowledges the new faculty seed grant from IIT Bombay. T. S. C. acknowledges support from the Ministry of Education Academic Research Fund Tier 1: RG5/22.

References

- 1 J. C. Védrine, Heterogeneous Catalysis on Metal Oxides, *Catalysts*, 2017, **7**(11), 341.
- 2 A. F. Lee, J. A. Bennett, J. C. Manayil and K. Wilson, Heterogeneous catalysis for sustainable biodiesel production via esterification and transesterification, *Chem. Soc. Rev.*, 2014, **43**(22), 7887–7916.
- 3 M. E. Günay and R. Yıldırım, Neural network Analysis of Selective CO Oxidation over Copper-Based Catalysts for Knowledge Extraction from Published Data in the Literature, *Ind. Eng. Chem. Res.*, 2011, **50**(22), 12488–12500.
- 4 A. Corma, *et al.*, Application of Artificial Neural Networks to Combinatorial Catalysis: Modeling and Predicting ODHE Catalysts, *ChemPhysChem*, 2002, **3**(11), 939–945.
- 5 L. Baumes, D. Farrusseng, M. Lengliz and C. Mirodatos, Using Artificial Neural Networks to Boost High-throughput Discovery in Heterogeneous Catalysis, *QSAR Comb. Sci.*, 2004, **23**(9), 767–778.
- 6 M. Suvarna, T. P. Araújo and J. Pérez-Ramírez, A generalized machine learning framework to predict the space-time yield of methanol from thermocatalytic CO₂ hydrogenation, *Appl. Catal., B*, 2022, **315**, 121530.
- 7 S. Shambhawi, G. Csányi and A. A. Lapkin, Active Learning Training Strategy for Predicting O Adsorption Free Energy on Perovskite Catalysts using Inexpensive Catalyst Features, *Chem.: Methods*, 2021, **1**(10), 444–450.
- 8 G. H. Gu, *et al.*, Practical Deep-Learning Representation for Fast Heterogeneous Catalyst Screening, *J. Phys. Chem. Lett.*, 2020, **11**(9), 3185–3191.
- 9 A. J. Chowdhury, *et al.*, Prediction of Adsorption Energies for Chemical Species on Metal Catalyst Surfaces Using Machine Learning, *J. Phys. Chem. C*, 2018, **122**(49), 28142–28150.
- 10 A. Zunger, Inverse design in search of materials with target functionalities, *Nat. Rev. Chem.*, 2018, **2**(4), 0121.

11 B. Sanchez-Lengeling and A. Aspuru-Guzik, Inverse molecular design using machine learning: Generative models for matter engineering, *Science*, 2018, **361**(6400), 360–365.

12 W. Xu and B. Yang, Microkinetic modeling with machine learning predicted binding energies of reaction intermediates of ethanol steam reforming: The limitations, *Mol. Catal.*, 2023, **537**, 112940.

13 S. Back, *et al.*, Convolutional Neural Network of Atomic Surface Structures To Predict Binding Energies for High-Throughput Screening of Catalysts, *J. Phys. Chem. Lett.*, 2019, **10**(15), 4401–4408.

14 J. K. Nørskov, T. Bligaard, J. Rossmeisl and C. H. Christensen, Towards the computational design of solid catalysts, *Nat. Chem.*, 2009, **1**(1), 37–46.

15 F. Studt, Grand Challenges in Computational Catalysis, *Front. Catal.*, 2021, **1**, 2673–7841.

16 O. Eisenstein and S. Shaik, Computational Catalysis: A Land of Opportunities, *Top. Catal.*, 2022, **65**(1), 1–5.

17 K. D. Vogiatzis, *et al.*, Computational Approach to Molecular Catalysis by 3d Transition Metals: Challenges and Opportunities, *Chem. Rev.*, 2019, **119**(4), 2453–2523.

18 J. C. Slater, A Simplification of the Hartree-Fock Method, *Phys. Rev.*, 1951, **81**(3), 385–390.

19 D. R. Hartree, The Wave Mechanics of an Atom with a Non-Coulomb Central Field. Part II. Some Results and Discussion, *Math. Proc. Cambridge Philos. Soc.*, 1928, **24**(1), 111–132.

20 C. Froese Fischer, General Hartree-Fock program, *Comput. Phys. Commun.*, 1987, **43**(3), 355–365.

21 C. David Sherrill and H. F. Schaefer, The Configuration Interaction Method: Advances in Highly Correlated Approaches, in *Advances in Quantum Chemistry*, ed. P.-O. Löwdin, J. R. Sabin, M. C. Zerner and E. Brändas, 1999, Academic Press, pp. 143–269.

22 J. Paldus, Chapter 7 - The beginnings of coupled-cluster theory: An eyewitness account, in *Theory and Applications of Computational Chemistry*, ed. C. E. Dykstra, G. Frenking, K. S. Kim and G. E. Scuseria, Elsevier, Amsterdam, 2005, pp. 115–147.

23 C. Møller and M. S. Plesset, Note on an Approximation Treatment for Many-Electron Systems, *Phys. Rev.*, 1934, **46**(7), 618–622.

24 P. Hohenberg and W. Kohn, Inhomogeneous Electron Gas, *Phys. Rev.*, 1964, **136**(3B), B864–B871.

25 W. Kohn and L. J. Sham, Self-Consistent Equations Including Exchange and Correlation Effects, *Phys. Rev.*, 1965, **140**(4A), A1133–A1138.

26 J. K. Nørskov, F. Abild-Pedersen, F. Studt and T. Bligaard, Density functional theory in surface chemistry and catalysis, *Proc. Natl. Acad. Sci. U. S. A.*, 2011, **108**(3), 937–943.

27 F. Jensen, Atomic orbital basis sets, *WIREs Comput. Mol. Sci.*, 2013, **3**(3), 273–295.

28 R. F. Stewart, Small Gaussian Expansions of Slater-Type Orbitals, *J. Chem. Phys.*, 2003, **52**(1), 431–438.

29 W. J. Hehre, R. F. Stewart and J. A. Pople, Self-Consistent Molecular-Orbital Methods. I. Use of Gaussian Expansions of Slater-Type Atomic Orbitals, *J. Chem. Phys.*, 2003, **51**(6), 2657–2664.

30 T. H. Dunning Jr., Gaussian basis sets for use in correlated molecular calculations. I. The atoms boron through neon and hydrogen, *J. Chem. Phys.*, 1989, **90**(2), 1007–1023.

31 M. J. Frisch, *et al.*, *Gaussian 16 Rev. C.01*, 2016, Wallingford, CT.

32 F. Neese, The ORCA program system, *WIREs Comput. Mol. Sci.*, 2012, **2**(1), 73–78.

33 M. S. Gordon and M. W. Schmidt, Chapter 41 - Advances in electronic structure theory: GAMESS a decade later, in *Theory and Applications of Computational Chemistry*, ed. C. E. Dykstra, G. Frenking, K. S. Kim and G. E. Scuseria, Elsevier, Amsterdam, 2005, pp. 1167–1189.

34 G. Kresse and J. Furthmüller, Efficient iterative schemes for ab initio total-energy calculations using a plane-wave basis set, *Phys. Rev. B: Condens. Matter Mater. Phys.*, 1996, **54**(16), 11169–11186.

35 N. Troullier and J. L. Martins, Efficient pseudopotentials for plane-wave calculations, *Phys. Rev. B: Condens. Matter Mater. Phys.*, 1991, **43**(3), 1993–2006.

36 G. Makov and M. C. Payne, Periodic boundary conditions in ab initio calculations, *Phys. Rev. B: Condens. Matter Mater. Phys.*, 1995, **51**(7), 4014–4022.

37 P. E. Blöchl, Projector augmented-wave method, *Phys. Rev. B: Condens. Matter Mater. Phys.*, 1994, **50**(24), 17953–17979.

38 G. Kresse and J. Furthmüller, Efficiency of ab-initio total energy calculations for metals and semiconductors using a plane-wave basis set, *Comput. Mater. Sci.*, 1996, **6**(1), 15–50.

39 P. Giannozzi, *et al.*, QUANTUM ESPRESSO: a modular and open-source software project for quantum simulations of materials, *J. Phys.: Condens. Matter*, 2009, **21**(39), 395502.

40 P. Giannozzi, *et al.*, Advanced capabilities for materials modelling with Quantum ESPRESSO, *J. Phys.: Condens. Matter*, 2017, **29**(46), 465901.

41 S. J. Clark, *et al.*, First principles methods using CASTEP, *Z. Kristallogr.*, 2005, **220**(5–6), 567–570.

42 R. Car and M. Parrinello, Unified Approach for Molecular Dynamics and Density-Functional Theory, *Phys. Rev. Lett.*, 1985, **55**(22), 2471–2474.

43 M. S. Tameh, A. K. Dearden and C. Huang, Accuracy of Density Functional Theory for Predicting Kinetics of Methanol Synthesis from CO and CO₂ Hydrogenation on Copper, *J. Phys. Chem. C*, 2018, **122**(31), 17942–17953.

44 P. J. Feibelman, *et al.*, The CO/Pt(111) Puzzle, *J. Phys. Chem. B*, 2001, **105**(18), 4018–4025.

45 J. P. Perdew, K. Burke and M. Ernzerhof, Generalized Gradient Approximation Made Simple, *Phys. Rev. Lett.*, 1996, **77**(18), 3865–3868.

46 B. Hammer, L. B. Hansen and J. K. Nørskov, Improved adsorption energetics within density-functional theory using revised Perdew-Burke-Ernzerhof functionals, *Phys. Rev. B: Condens. Matter Mater. Phys.*, 1999, **59**(11), 7413–7421.

47 K. Burke, J. P. Perdew and Y. Wang, Derivation of a Generalized Gradient Approximation: The PW91 Density Functional, in *Electronic Density Functional Theory: Recent Progress and New Directions*, ed. J. F. Dobson, G. Vignale and M. P. Das, Springer US, Boston, MA, 1998, pp. 81–111.

48 J. Klimeš, D. R. Bowler and A. Michaelides, Chemical accuracy for the van der Waals density functional, *J. Phys.: Condens. Matter*, 2010, **22**(2), 022201.

49 L. C. Grabow and M. Mavrikakis, Mechanism of Methanol Synthesis on Cu through CO₂ and CO Hydrogenation, *ACS Catal.*, 2011, **1**(4), 365–384.

50 Y.-F. Zhao, *et al.*, Insight into methanol synthesis from CO₂ hydrogenation on Cu(111): Complex reaction network and the effects of H₂O, *J. Catal.*, 2011, **281**(2), 199–211.

51 F. Muttaqien, *et al.*, CO₂ adsorption on the copper surfaces: van der Waals density functional and TPD studies, *J. Chem. Phys.*, 2017, **147**(9), 094702.

52 O. Mohan, Q. T. Trinh, A. Banerjee and S. H. Mushrif, Predicting CO₂ adsorption and reactivity on transition metal surfaces using popular density functional theory methods, *Mol. Simul.*, 2019, 1–10.

53 S. Grimme, J. Antony, S. Ehrlich and H. Krieg, A consistent and accurate ab initio parametrization of density functional dispersion correction (DFT-D) for the 94 elements H–Pu, *J. Chem. Phys.*, 2010, **132**(15), 154104.

54 S. Grimme, S. Ehrlich and L. Goerigk, Effect of the damping function in dispersion corrected density functional theory, *J. Comput. Chem.*, 2011, **32**(7), 1456–1465.

55 A. Tkatchenko and M. Scheffler, Accurate Molecular Van Der Waals Interactions from Ground-State Electron Density and Free-Atom Reference Data, *Phys. Rev. Lett.*, 2009, **102**(7), 073005.

56 V. I. Anisimov, J. Zaanen and O. K. Andersen, Band theory and Mott insulators: Hubbard U instead of Stoner I, *Phys. Rev. B: Condens. Matter Mater. Phys.*, 1991, **44**(3), 943–954.

57 L. Wang, T. Maxisch and G. Ceder, Oxidation energies of transition metal oxides within the GGA + U framework, *Phys. Rev. B: Condens. Matter Mater. Phys.*, 2006, **73**(19), 195107.

58 K. Bhola, *et al.*, Influence of Hubbard U Parameter in Simulating Adsorption and Reactivity on CuO: Combined Theoretical and Experimental Study, *J. Phys. Chem. C*, 2017, **121**(39), 21343–21353.

59 Q. T. Trinh, *et al.*, Synergistic Application of XPS and DFT to Investigate Metal Oxide Surface Catalysis, *J. Phys. Chem. C*, 2018, **122**(39), 22397–22406.

60 J. Kapil, P. Shukla and A. Pathak, Review Article on Density Functional Theory, *Recent Trends in Materials and Devices*, Springer Singapore, Singapore, 2020.

61 P. Makkar and N. N. Ghosh, A review on the use of DFT for the prediction of the properties of nanomaterials, *RSC Adv.*, 2021, **11**(45), 27897–27924.

62 M. Elstner, *et al.*, Self-consistent-charge density-functional tight-binding method for simulations of complex materials properties, *Phys. Rev. B: Condens. Matter Mater. Phys.*, 1998, **58**(11), 7260–7268.

63 M. Gaus, Q. Cui and M. Elstner, DFTB3: Extension of the Self-Consistent-Charge Density-Functional Tight-Binding Method (SCC-DFTB), *J. Chem. Theory Comput.*, 2011, **7**(4), 931–948.

64 M. Elstner, SCC-DFTB: What Is the Proper Degree of Self-Consistency?, *J. Phys. Chem. A*, 2007, **111**(26), 5614–5621.

65 M. Van den Bossche, H. Grönbeck and B. Hammer, Tight-Binding Approximation-Enhanced Global Optimization, *J. Chem. Theory Comput.*, 2018, **14**(5), 2797–2807.

66 M. Van den Bossche, DFTB-Assisted Global Structure Optimization of 13- and 55-Atom Late Transition Metal Clusters, *J. Phys. Chem. A*, 2019, **123**(13), 3038–3045.

67 Y. Zhou, *et al.*, Multilayer stabilization for fabricating high-loading single-atom catalysts, *Nat. Commun.*, 2020, **11**(1), 5892.

68 M. Gruden, Benchmarking density functional tight binding models for barrier heights and reaction energetics of organic molecules, *J. Comput. Chem.*, 2017, **38**(25), 2171–2185.

69 G. Zheng, S. Irle and K. Morokuma, Performance of the DFTB method in comparison to DFT and semiempirical methods for geometries and energies of C₂₀–C₈₆ fullerene isomers, *Chem. Phys. Lett.*, 2005, **412**(1), 210–216.

70 F. Spiegelman, *et al.*, Density-functional tight-binding: basic concepts and applications to molecules and clusters, *Adv. Phys.: X*, 2020, **5**(1), 1710252.

71 E. Shustorovich and H. Sellers, The UBI-QEP method: A practical theoretical approach to understanding chemistry on transition metal surfaces, *Surf. Sci. Rep.*, 1998, **31**(1), 1–119.

72 E. Shustorovich and A. T. Bell, An analysis of methanol synthesis from CO and CO₂ on Cu and Pd surfaces by the bond-order-conservation-Morse-potential approach, *Surf. Sci.*, 1991, **253**(1), 386–394.

73 E. Shustorovich and A. T. Bell, An analysis of Fischer-Tropsch synthesis by the bond-order-conservation-Morse-potential approach, *Surf. Sci.*, 1991, **248**(3), 359–368.

74 K. H. Delgado, *et al.*, Surface Reaction Kinetics of Steam- and CO₂-Reforming as Well as Oxidation of Methane over Nickel-Based Catalysts, *Catalysts*, 2015, **5**(2), 871–904.

75 T. P. Senftle, *et al.*, The ReaxFF reactive force-field: development, applications and future directions, *npj Comput. Mater.*, 2016, **2**(1), 15011.

76 A. C. T. van Duin, S. Dasgupta, F. Lorant and W. A. Goddard, ReaxFF: A Reactive Force Field for Hydrocarbons, *J. Phys. Chem. A*, 2001, **105**(41), 9396–9409.

77 J. Ludwig, D. G. Vlachos, A. C. T. van Duin and W. A. Goddard, Dynamics of the Dissociation of Hydrogen on Stepped Platinum Surfaces Using the ReaxFF Reactive Force Field, *J. Phys. Chem. B*, 2006, **110**(9), 4274–4282.

78 C. Zou, A. C. T. van Duin and D. C. Sorescu, Theoretical investigation of Hydrogen Adsorption and dissociation on Iron and Iron Carbide Surfaces using the ReaxFF force Field Method, *Top. Catal.*, 2012, **55**(5), 391–401.

79 K. D. Nielson, *et al.*, Development of the ReaxFF Reactive Force Field for Describing Transition Metal Catalyzed Reactions, with Application to the Initial Stages of the Catalytic Formation of Carbon Nanotubes, *J. Phys. Chem. A*, 2005, **109**(3), 493–499.

80 J. E. Mueller, A. C. T. van Duin and W. A. Goddard, Development and Validation of ReaxFF Reactive Force Field for Hydrocarbon Chemistry Catalyzed by Nickel, *J. Phys. Chem. C*, 2010, **114**(11), 4939–4949.

81 K. Chenoweth, *et al.*, Development and Application of a ReaxFF Reactive Force Field for Oxidative Dehydrogenation on Vanadium Oxide Catalysts, *J. Phys. Chem. C*, 2008, **112**(37), 14645–14654.

82 K. Chenoweth, A. C. T. van Duin and W. A. Goddard III, The ReaxFF Monte Carlo Reactive Dynamics Method for Predicting Atomistic Structures of Disordered Ceramics: Application to the Mo₃VO_x Catalyst, *Angew. Chem., Int. Ed.*, 2009, **48**(41), 7630–7634.

83 L. Wu, *et al.*, Stabilizing mechanism of single-atom catalysts on a defective carbon surface, *npj Comput. Mater.*, 2020, **6**(1), 23.

84 X.-Q. Zhang, *et al.*, Site Stability on Cobalt Nanoparticles: A Molecular Dynamics ReaxFF Reactive Force Field Study, *J. Phys. Chem. C*, 2014, **118**(13), 6882–6886.

85 W. Guichang, Y. Wenqi, W. Jie and Q. Yuanyuan, Reactive Force Field Model Molecular Dynamics Study on the Thermal Stability of Single Atom Alloy Catalysts, *Xinyang Shifan Xueyuan Xuebao, Ziran Kexueban*, 2020, **33**(2), 191.

86 J. J. P. Stewart, MOPAC: A semiempirical molecular orbital program, *J. Comput.-Aided Mol. Des.*, 1990, **4**(1), 1–103.

87 S. W. Benson and J. H. Buss, Additivity Rules for the Estimation of Molecular Properties. Thermodynamic Properties, *J. Chem. Phys.*, 1958, **29**(3), 546–572.

88 C. W. Gao, J. W. Allen, W. H. Green and R. H. West, Reaction Mechanism Generator: Automatic construction of chemical kinetic mechanisms, *Comput. Phys. Commun.*, 2016, **203**, 212–225.

89 C. F. Goldsmith and R. H. West, Automatic Generation of Microkinetic Mechanisms for Heterogeneous Catalysis, *J. Phys. Chem. C*, 2017, **121**(18), 9970–9981.

90 W. Thiel, Semiempirical quantum-chemical methods, *WIREs Comput. Mol. Sci.*, 2014, **4**(2), 145–157.

91 T. Liang, *et al.*, Reactive Potentials for Advanced Atomistic Simulations, *Annu. Rev. Mater. Res.*, 2013, **43**(1), 109–129.

92 S. Maeda, T. Taketsugu and K. Morokuma, Exploring transition state structures for intramolecular pathways by the artificial force induced reaction method, *J. Comput. Chem.*, 2014, **35**(2), 166–173.

93 P. M. Zimmerman, Automated discovery of chemically reasonable elementary reaction steps, *J. Comput. Chem.*, 2013, **34**(16), 1385–1392.

94 Q. Zhao and B. M. Savoie, Simultaneously improving reaction coverage and computational cost in automated reaction prediction tasks, *Nat. Comput. Sci.*, 2021, **1**(7), 479–490.

95 M. Liu, *et al.*, Reaction Mechanism Generator v3.0: Advances in Automatic Mechanism Generation, *J. Chem. Inf. Model.*, 2021, **61**(6), 2686–2696.

96 S. Rangarajan, R. R. O. Brydon, A. Bhan and P. Daoutidis, Automated identification of energetically feasible mechanisms of complex reaction networks in heterogeneous catalysis: application to glycerol conversion on transition metals, *Green Chem.*, 2014, **16**(2), 813–823.

97 D. A. Simonetti, E. L. Kunkes and J. A. Dumesic, Gas-phase conversion of glycerol to synthesis gas over carbon-supported platinum and platinum-rhenium catalysts, *J. Catal.*, 2007, **247**(2), 298–306.

98 E. P. Maris and R. J. Davis, Hydrogenolysis of glycerol over carbon-supported Ru and Pt catalysts, *J. Catal.*, 2007, **249**(2), 328–337.

99 K. H. Delgado, Surface Reaction Kinetics of Steam- and CO₂-Reforming as Well as Oxidation of Methane over Nickel-Based Catalysts, *Catalysts*, 2015, **5**(2), 871–904.

100 C. T. Campbell, The Degree of Rate Control: A Powerful Tool for Catalysis Research, *ACS Catal.*, 2017, **7**(4), 2770–2779.

101 Shambhavi, J. M. Weber and A. A. Lapkin, Micro-kinetics analysis based on partial reaction networks to compare catalysts performances for methane dry reforming reaction, *Chem. Eng. J.*, 2023, 143212.

102 A. H. Motagamwala and J. A. Dumesic, Microkinetic Modeling: A Tool for Rational Catalyst Design, *Chem. Rev.*, 2021, **121**(2), 1049–1076.

103 Z. Wang and P. Hu, Towards rational catalyst design: a general optimization framework, *Philos. Trans. R. Soc., A*, 2016, **374**(2061), 20150078.

104 S. Rangarajan, C. T. Maravelias and M. Mavrikakis, Sequential-Optimization-Based Framework for Robust Modeling and Design of Heterogeneous Catalytic Systems, *J. Phys. Chem. C*, 2017, **121**(46), 25847–25863.

105 T. Le, V. C. Epa, F. R. Burden and D. A. Winkler, Quantitative Structure–Property Relationship Modeling of Diverse Materials Properties, *Chem. Rev.*, 2012, **112**(5), 2889–2919.

106 A. J. Medford, *et al.*, CatMAP: A Software Package for Descriptor-Based Microkinetic Mapping of Catalytic Trends, *Catal. Lett.*, 2015, **145**(3), 794–807.

107 C. A. Wolcott, A. J. Medford, F. Studt and C. T. Campbell, Degree of rate control approach to computational catalyst screening, *J. Catal.*, 2015, **330**, 197–207.

108 J. K. Nørskov, T. Bligaard and J. Kleis, Rate Control and Reaction Engineering, *Science*, 2009, **324**(5935), 1655–1656.

109 O. Mohan, *et al.*, Investigating CO₂ Methanation on Ni and Ru: DFT Assisted Microkinetic Analysis, *ChemCatChem*, 2021, **13**(10), 2420–2433.

110 P. Sabatier, *La catalyse en chimie organique*, 1920.

111 M. T. Darby, M. Stamatakis, A. Michaelides and E. C. H. Sykes, Lonely Atoms with Special Gifts: Breaking Linear Scaling Relationships in Heterogeneous Catalysis with Single-Atom Alloys, *J. Phys. Chem. Lett.*, 2018, **9**(18), 5636–5646.

112 S. M. Stratton, S. Zhang and M. M. Montemore, Addressing complexity in catalyst design: From volcanoes and scaling to more sophisticated design strategies, *Surf. Sci. Rep.*, 2023, **78**(3), 100597.

113 A. Chandrasekaran, *et al.*, Solving the electronic structure problem with machine learning, *npj Comput. Mater.*, 2019, **5**(1), 22.

114 T. Toyao, *et al.*, Toward Effective Utilization of Methane: Machine Learning Prediction of Adsorption Energies on Metal Alloys, *J. Phys. Chem. C*, 2018, **122**(15), 8315–8326.

115 A. A. Peterson, Acceleration of saddle-point searches with machine learning, *J. Chem. Phys.*, 2016, **145**(7), 074106.

116 O.-P. Koistinen, Nudged elastic band calculations accelerated with Gaussian process regression, *J. Chem. Phys.*, 2017, **147**(15), 152720.

117 X. Ma, Z. Li, L. E. K. Achenie and H. Xin, Machine-Learning-Augmented Chemisorption Model for CO₂ Electroreduction Catalyst Screening, *J. Phys. Chem. Lett.*, 2015, **6**(18), 3528–3533.

118 F. Guo, *et al.*, Intelligent-ReaxFF: Evaluating the reactive force field parameters with machine learning, *Comput. Mater. Sci.*, 2020, **172**, 109393.

119 Z. Li, *et al.*, High-throughput screening of bimetallic catalysts enabled by machine learning, *J. Mater. Chem. A*, 2017, **5**(46), 24131–24138.

120 L. Ward, A. Agrawal, A. Choudhary and C. Wolverton, A general-purpose machine learning framework for predicting properties of inorganic materials, *npj Comput. Mater.*, 2016, **2**(1), 16028.

121 B. Meredig, *et al.*, Combinatorial screening for new materials in unconstrained composition space with machine learning, *Phys. Rev. B: Condens. Matter Mater. Phys.*, 2014, **89**(9), 094104.

122 T. Xie and J. C. Grossman, Crystal Graph Convolutional Neural Networks for an Accurate and Interpretable Prediction of Material Properties, *Phys. Rev. Lett.*, 2018, **120**(14), 145301.

123 P. Villars, *et al.*, Data-driven atomic environment prediction for binaries using the Mendeleev number: Part 1. Composition AB, *J. Alloys Compd.*, 2004, **367**(1), 167–175.

124 M. Andersen, S. V. Levchenko, M. Scheffler and K. Reuter, Beyond Scaling Relations for the Description of Catalytic Materials, *ACS Catal.*, 2019, **9**(4), 2752–2759.

125 J. Dean, M. G. Taylor and G. Mpourmpakis, Unfolding adsorption on metal nanoparticles: Connecting stability with catalysis, *Sci. Adv.*, 2019, **5**(9), eaax5101.

126 H. Xin, A. Holewinski and S. Linic, Predictive Structure-Reactivity Models for Rapid Screening of Pt-Based Multimetallic Electrocatalysts for the Oxygen Reduction Reaction, *ACS Catal.*, 2012, **2**(1), 12–16.

127 J. Noh, S. Back, J. Kim and Y. Jung, Active learning with non-ab initio input features toward efficient CO₂ reduction catalysts, *Chem. Sci.*, 2018, **9**(23), 5152–5159.

128 K. T. Schütt, *et al.*, How to represent crystal structures for machine learning: Towards fast prediction of electronic properties, *Phys. Rev. B: Condens. Matter Mater. Phys.*, 2014, **89**(20), 205118.

129 D. Wu, C. Dong, H. Zhan and X.-W. Du, Bond-Energy-Integrated Descriptor for Oxygen Electrocatalysis of Transition Metal Oxides, *J. Phys. Chem. Lett.*, 2018, **9**(12), 3387–3391.

130 F. Calle-Vallejo, *et al.*, Fast Prediction of Adsorption Properties for Platinum Nanocatalysts with Generalized Coordination Numbers, *Angew. Chem. Int. Ed.*, 2014, **53**(32), 8316–8319.

131 X. Ma and H. Xin, Orbitalwise Coordination Number for Predicting Adsorption Properties of Metal Nanocatalysts, *Phys. Rev. Lett.*, 2017, **118**(3), 036101.

132 Y.-L. Lee, *et al.*, Prediction of solid oxide fuel cell cathode activity with first-principles descriptors, *Energy Environ. Sci.*, 2011, **4**(10), 3966–3970.

133 J. Suntivich, *et al.*, A Perovskite Oxide Optimized for Oxygen Evolution Catalysis from Molecular Orbital Principles, *Science*, 2011, **334**(6061), 1383–1385.

134 H. Xin, *et al.*, Effects of \$d\$-band shape on the surface reactivity of transition-metal alloys, *Phys. Rev. B: Condens. Matter Mater. Phys.*, 2014, **89**(11), 115114.

135 T. S. Choksi, L. T. Roling, V. Streibel and F. Abild-Pedersen, Predicting Adsorption Properties of Catalytic Descriptors on Bimetallic Nanoalloys with Site-Specific Precision, *J. Phys. Chem. Lett.*, 2019, **10**(8), 1852–1859.

136 Y. Zhang and C. Ling, A strategy to apply machine learning to small datasets in materials science, *npj Comput. Mater.*, 2018, **4**(1), 25.

137 Z. Li, L. E. K. Achenie and H. Xin, An Adaptive Machine Learning Strategy for Accelerating Discovery of Perovskite Electrocatalysts, *ACS Catal.*, 2020, **10**(7), 4377–4384.

138 Z. Li, X. Ma and H. Xin, Feature engineering of machine-learning chemisorption models for catalyst design, *Catal. Today*, 2017, **280**, 232–238.

139 W. A. Harrison and S. Froyen, Universal linear-combination-of-atomic-orbitals parameters for \$d\$-state solids, *Phys. Rev. B: Condens. Matter Mater. Phys.*, 1980, **21**(8), 3214–3221.

140 J. S. Hummelshøj, *et al.*, CatApp: A Web Application for Surface Chemistry and Heterogeneous Catalysis, *Angew. Chem.*, 2012, **124**(1), 278–280.

141 K. T. Winther, *et al.*, Catalysis-Hub.org, an open electronic structure database for surface reactions, *Sci. Data*, 2019, **6**(1), 75.

142 O. Mamun, K. T. Winther, J. R. Boes and T. Bligaard, High-throughput calculations of catalytic properties of bimetallic alloy surfaces, *Sci. Data*, 2019, **6**(1), 76.

143 L. Chanussoot, A. Das, S. Goyal, T. Lavril, M. Shuaibi, M. Riviere, K. Tran, J. Heras-Domingo, C. Ho, W. Hu, A. Palizhati, A. Sriram, B. Wood, J. Yoon, D. Parikh, C. L. Zitnick and Z. Ulissi, Open Catalyst 2020 (OC20) Dataset and Community Challenges, *ACS Catal.*, 2021, **11**(10), 6059–6072.

144 A. Jain, Commentary: The Materials Project: A materials genome approach to accelerating materials innovation, *APL Mater.*, 2013, **1**(1), 011002.

145 A. Jain, *et al.*, Commentary: The Materials Project: A materials genome approach to accelerating materials innovation, *APL Mater.*, 2013, **1**(1), 011002.

146 K. Tran and Z. W. Ulissi, Active learning across intermetallics to guide discovery of electrocatalysts for CO₂ reduction and H₂ evolution, *Nat. Catal.*, 2018, **1**(9), 696–703.

147 R. A. Hoyt, *et al.*, Machine Learning Prediction of H Adsorption Energies on Ag Alloys, *J. Chem. Inf. Model.*, 2019, **59**(4), 1357–1365.

148 M. M. Montemore and J. W. Medlin, Scaling relations between adsorption energies for computational screening and design of catalysts, *Catal. Sci. Technol.*, 2014, **4**(11), 3748–3761.

149 O. Mamun, K. T. Winther, J. R. Boes and T. Bligaard, A Bayesian framework for adsorption energy prediction on bimetallic alloy catalysts, *npj Comput. Mater.*, 2020, **6**(1), 177.

150 K. Tran, *et al.*, Methods for comparing uncertainty quantifications for material property predictions, *Mach. Learn.: Sci. Technol.*, 2020, **1**(2), 025006.

151 L. Chanussot, *et al.*, Open Catalyst 2020 (OC20) Dataset and Community Challenges, *ACS Catal.*, 2021, **11**(10), 6059–6072.

152 J. W. Lee and C. Giraud-Carrier, Transfer Learning in Decision Trees in 2007 International Joint Conference on Neural Networks, 2007.

153 B. Zhang, *et al.*, Transfer learning-based online multiperson tracking with Gaussian process regression, *Concurr. Comput. Pract. Exp.*, 2018, **30**(23), e4917.

154 O. T. Unke, *et al.*, Machine Learning Force Fields, *Chem. Rev.*, 2021, **121**(16), 10142–10186.

155 V. L. Deringer, M. A. Caro and G. Csányi, Machine Learning Interatomic Potentials as Emerging Tools for Materials Science, *Adv. Mater.*, 2019, 1902765.

156 A. P. Bartók, R. Kondor and G. Csányi, On representing chemical environments, *Phys. Rev. B: Condens. Matter Mater. Phys.*, 2013, **87**(18), 184115.

157 A. P. Bartók, J. Kermode, N. Bernstein and G. Csányi, Machine Learning a General-Purpose Interatomic Potential for Silicon, *Phys. Rev. X*, 2018, **8**(4), 041048.

158 V. L. Deringer and G. Csányi, Machine learning based interatomic potential for amorphous carbon, *Phys. Rev. B*, 2017, **95**(9), 094203.

159 W. J. Szlachta, A. P. Bartók and G. Csányi, Accuracy and transferability of Gaussian approximation potential models for tungsten, *Phys. Rev. B: Condens. Matter Mater. Phys.*, 2014, **90**(10), 104108.

160 H. Muhli, *et al.*, Machine learning force fields based on local parametrization of dispersion interactions: Application to the phase diagram of C₆₀, *Phys. Rev. B*, 2021, **104**(5), 054106.

161 L. L. Schaaf, E. Fako and S. De, *et al.*, Accurate energy barriers for catalytic reaction pathways: an automatic training protocol for machine learning force fields, *npj Comput. Mater.*, 2023, **9**(1), 180.

162 F. Abild-Pedersen, *et al.*, Scaling Properties of Adsorption Energies for Hydrogen-Containing Molecules on Transition-Metal Surfaces, *Phys. Rev. Lett.*, 2007, **99**(1), 016105.

163 J. Greeley, Theoretical Heterogeneous Catalysis: Scaling Relationships and Computational Catalyst Design, *Annu. Rev. Chem. Biomol. Eng.*, 2016, **7**(1), 605–635.

164 F. Calle-Vallejo, D. Loffreda, M. T. M. Koper and P. Sautet, Introducing structural sensitivity into adsorption–energy scaling relations by means of coordination numbers, *Nat. Chem.*, 2015, **7**(5), 403–410.

165 M. G. Evans and M. Polanyi, *J. Chem. Soc., Faraday Trans.*, 1936, **32**, 1333–1360.

166 C. Fan, Origin of synergistic effect over Ni-based bimetallic surfaces: A density functional theory study, *J. Chem. Phys.*, 2012, **137**(1), 014703.

167 Y. Huang, *et al.*, Methane dehydrogenation on Au/Ni surface alloys – a first-principles study, *Catal. Sci. Technol.*, 2013, **3**(5), 1343–1354.

168 J. Rossmeisl, *et al.*, Electrolysis of water on oxide surfaces, *J. Electroanal. Chem.*, 2007, **607**(1), 83–89.

169 T. Choksi, P. Majumdar and J. P. Greeley, Electrostatic Origins of Linear Scaling Relationships at Bifunctional Metal/Oxide Interfaces: A Case Study of Au Nanoparticles on Doped MgO Substrates, *Angew. Chem., Int. Ed.*, 2018, **57**(47), 15410–15414.

170 A. Logadottir, *et al.*, The Brønsted–Evans–Polanyi Relation and the Volcano Plot for Ammonia Synthesis over Transition Metal Catalysts, *J. Catal.*, 2001, **197**(2), 229–231.

171 Q. Gao, *et al.*, Breaking adsorption-energy scaling limitations of electrocatalytic nitrate reduction on intermetallic CuPd nanocubes by machine-learned insights, *Nat. Commun.*, 2022, **13**(1), 2338.

172 C. J. Bartel, *et al.*, A critical examination of compound stability predictions from machine-learned formation energies, *npj Comput. Mater.*, 2020, **6**(1), 97.

